and 40 mice were used for survival study and for biological and histological analysis, respectively. The mutant mice were bred and kept in specific pathogen-free conditions in the Center for Animal Resources and Development (CARD), Kumamoto University. Animals were housed in cages in a room under controlled conditions at 24 °C with a 12-h light cycle and given free access to food and water. All experimental procedures conformed to the animal use guidelines of the Committee for Ethics on Animal Experiments of Kumamoto University (approval numbers M24-367).

In our preliminary study, we examined the effects of 4000 to 10,000 mg/kg of HPBCD on the parameters used in this study, such as survival rate, serum biochemical parameters, and histological changes in *Npc1* mutant mice. However, significant changes were not observed at these doses. Therefore, we chose a dose of 20,000 mg/kg of HPBCD in this study. In the saline-treated groups, saline was subcutaneous injected instead of HPBCD solution. In the survival study, mice were divided into the following groups: (1) HPBCD-treated $Npc1^{+/+}$ group ($n = 12$) (2) HPBCD-treated $Npc1^{+/-}$ group ($n = 12$), and (3) HPBCD-treated $Npc1^{-/-}$ group ($n = 11$) and were monitored for 72 h after the injection. In the biological and histological analysis, mice were divided into the following groups: (1) saline-treated $Npc1^{+/+}$ group ($n = 7$); (2) HPBCD-treated $Npc1^{+/+}$ group ($n = 7$); (3) saline-treated $Npc1^{+/-}$ group ($n = 7$); (4) HPBCD-treated $Npc1^{+/-}$ group ($n = 7$); (5) saline-treated $Npc1^{-/-}$ group ($n = 5$); and (6) HPBCD-treated $Npc1^{-/-}$ group ($n = 7$). In the HPBCD-treated groups, HPBCD was dissolved in water and adjusted to pH 7.4 and administered by a subcutaneous injection through the back of the neck in mice at a dose of 20,000 mg/kg. For measurements of biochemical parameters and histological analysis, mice were euthanized 8 h after the injection, and blood and organ samples were collected.

2.3. Measurement of serum biochemical parameters

Blood samples, collected from the inferior vena cava at 8 h after the HPBCD injection, were immediately centrifuged at 4000 ×g at 4 °C for 10 min, and sera were collected. Alanine aminotransferase (ALT) and creatinine were measured using a bio-analyzer (SPOTCHEM EZ SP-4430; ARKRAY, Inc., Kyoto, Japan).

2.4. Histological analysis

Tissue samples were fixed in 10% neutral buffered formalin and then embedded in paraffin before being cut into 4-mm-thick sections. For histological examination of the liver and lung, sections were stained first with Mayer's hematoxylin and then with 1% eosin alcohol solution. For histological examination of the kidney, sections were stained with periodic acid-Schiff stain. Samples were mounted with malinol and inspected using a light microscope (Biorevo; Keyence Co., Osaka, Japan). Lung injury score was determined macroscopically by an observer unaware of the treatment the mice had received. According to a previously reported method [11], the lung injury score was scored as follows: 0 (no damage) to 4+ (maximal damage) according to the combined assessments of alveolar congestion, hemorrhage, infiltration/aggregation of inflammatory cells in

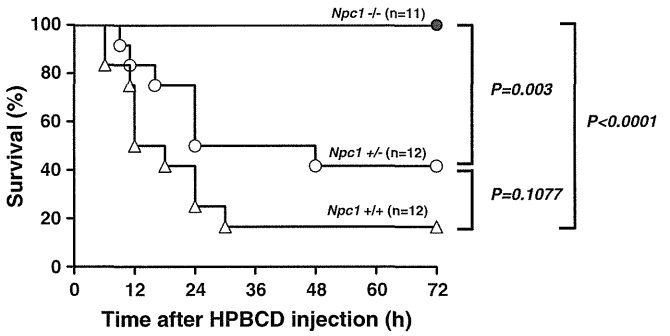

Fig. 1. Effect of HPBCD injection on survival rate of *Npc1* mutant mice. $Npc1^{+/+}$ ($n = 12$), $Npc1^{+/-}$ ($n = 12$) and $Npc1^{-/-}$ ($n = 11$) mice were administered HPBCD (20,000 mg/kg) subcutaneously and monitored for 72 h.

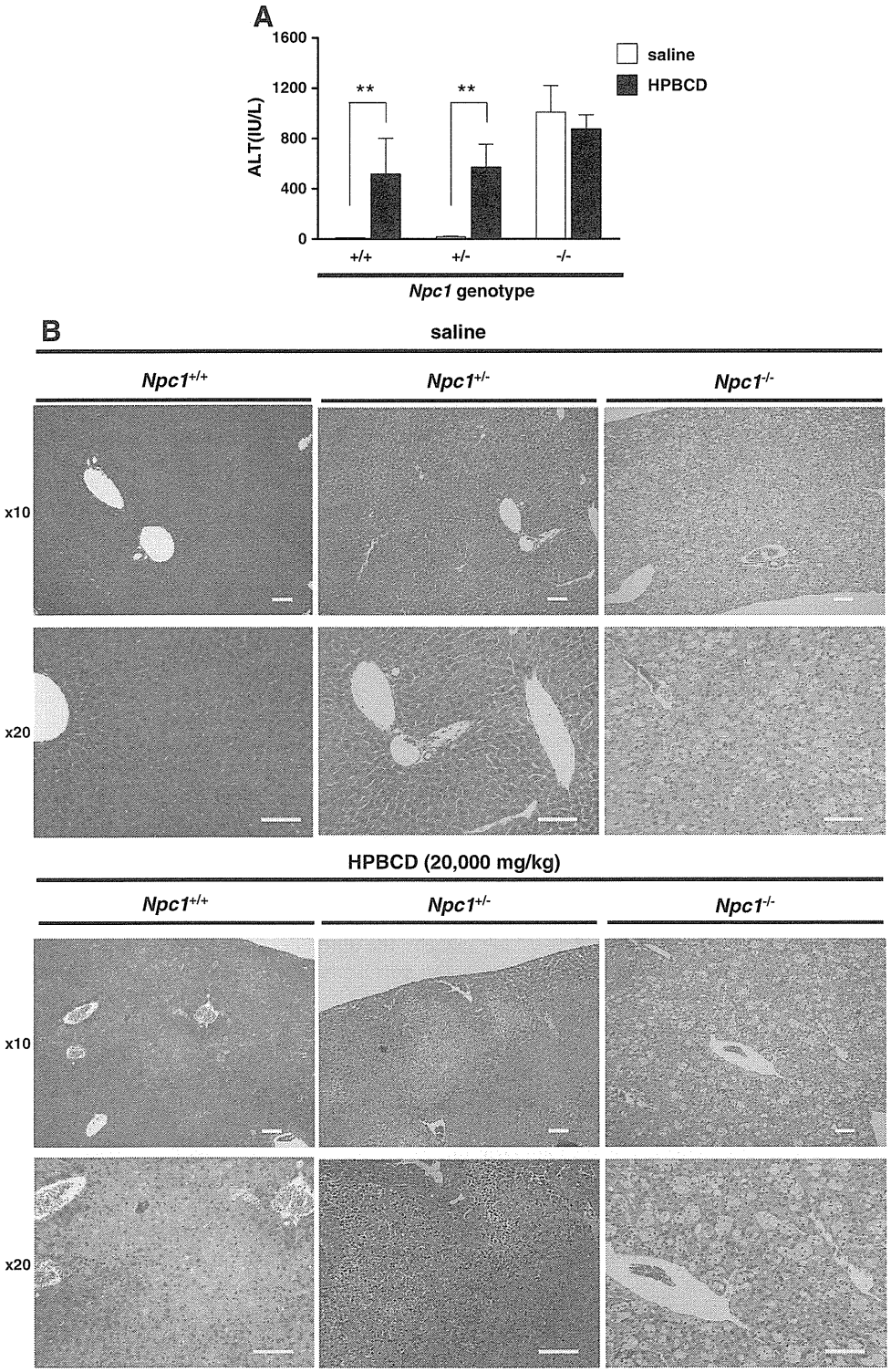
A
1600
1200
800
400
0
ALT(IU/L)
**
**
saline
HPBCD
+/+
+/-
-/-
Npc1 genotype
B
saline
Npc1+/+
Npc1+/-
Npc1-/-
x10
x20
HPBCD (20,000 mg/kg)
Npc1+/+
Npc1+/-
Npc1-/-
x10
x20

the airspace or vessel wall, and thickness of the alveolar wall. Histological analysis, including the lung injury score, was determined by light microscopy by three independent observers. The assignment of study groups was blinded to the observers.

2.5. Cell culture and measurement of cytotoxicity

Wild-type and *Npc1* null Chinese hamster ovary (CHO) cells that we previously developed [12] were used in this study. The cells were grown in culture medium consisting of a 1:1 mixture of DMEM/F12 supplemented with 10% FBS. Cells were maintained at 37 °C in a saturated humidity atmosphere of 95% air and 5% CO_2.

To evaluate the cytotoxic effects of HPBCD, assays to measure cell viability and cell death were performed. HPBCD-induced cell injury was evaluated by a cell viability assay using mitochondrial dehydrogenase activity and by a calcein-acetomethoxy and propidium iodide (calcein-AM and PI stain viable and dead cells, respectively) dual-staining assay. Mitochondrial dehydrogenase activity was measured using a modified MTT assay, namely the water-soluble tetrazolium salt (WST-8) assay, using a Cell Counting Kit according to the manufacturer's protocol. Calcein-AM/PI co-staining was performed using the Cellstain® Double Staining Kit. CHO cells were incubated in 96-well plates (1×10^4 cells/well) in culture medium at 37 °C for 24 h. After 24 h to allow cells to adhere, the medium was replaced with fresh medium containing HPBCD (0–80 mM) without FBS for 3 h and then incubated with the WST-8 solution for 1.5 h at 37 °C. The maximum absorption of the WST-8 formazan (450 nm) was measured using a micro plate reader (Tecan Co., Ltd, Männedorf, Switzerland). Cell viability was expressed as a percentage of the viable cells relative to the untreated controls. Cells were incubated with calcein-AM and 0.4 mmol/L PI in phosphate-buffered saline for 15 min. Cell death was observed by measuring the fluorescence of calcein-AM and PI at excitation/emission wavelengths of 490/510 nm and 530/580 nm, respectively, using a fluorescence microscope (Biorevo; Keyence, Osaka, Japan).

2.6. Statistical analysis

Statistical analysis was performed using GraphPad Prism ver. 5.01 (GraphPad Software, San Diego, CA, USA). Analysis of the histological score was also performed. Survival data were analyzed using the Kaplan–Meier method, and the log-rank test was used to compare statistical significances. Multiple comparisons were conducted to examine the statistical significance of the results. When uniform variance of the result was identified by Bartlett's analysis ($p < 0.05$), one-way analysis of variance was used to test for significant differences. When significant differences ($p < 0.05$) were identified, the results were further analyzed by the Dunnett's or Tukey's multiple range test for significant differences among the values. If uniform variance of the result was not identified, non-parametric multiple comparisons were made. After confirming significant differences ($p < 0.05$) using the Kruskal–Wallis analysis, the differences were then examined using the Dunnett's test. Analysis of histological score was also performed using these nonparametric multiple comparison tests.

3. Results

3.1. Survival rate of wild type and Npc1 mutant mice treated with a toxic dose of HPBCD

We examined the effects of subcutaneously injected 20,000 mg/kg of HPBCD on survival in *Npc1* mutant mice. Over half of the mice of the $Npc1^{+/+}$ or $Npc1^{+/-}$ groups were dead within 72 h by an administration of HPBCD (Fig. 1). Stress responses, such as anorexia and fluffing and withering of the fur, were observed in the surviving mice of the wild-type and $Npc1^{+/-}$ groups. In contrast, all of the $Npc1^{-/-}$ mice survived, and stress responses exhibited by the $Npc1^{+/-}$ mice were not observed. In the Kaplan–

Fig. 2. Hepatic biochemical and histological analysis of wild-type and *Npc1* mutant mice treated with a toxic dose of HPBCD. Serum ALT levels (A) and representative hepatic sections (hematoxylin eosin stained) (B) 8 h after saline or HPBCD (20,000 mg/kg) subcutaneous injection. Values are the mean ± S.E.M., ($n = 5$–7). ** $P < 0.01$; n.s., not significant. Scale bar = 400 μm.

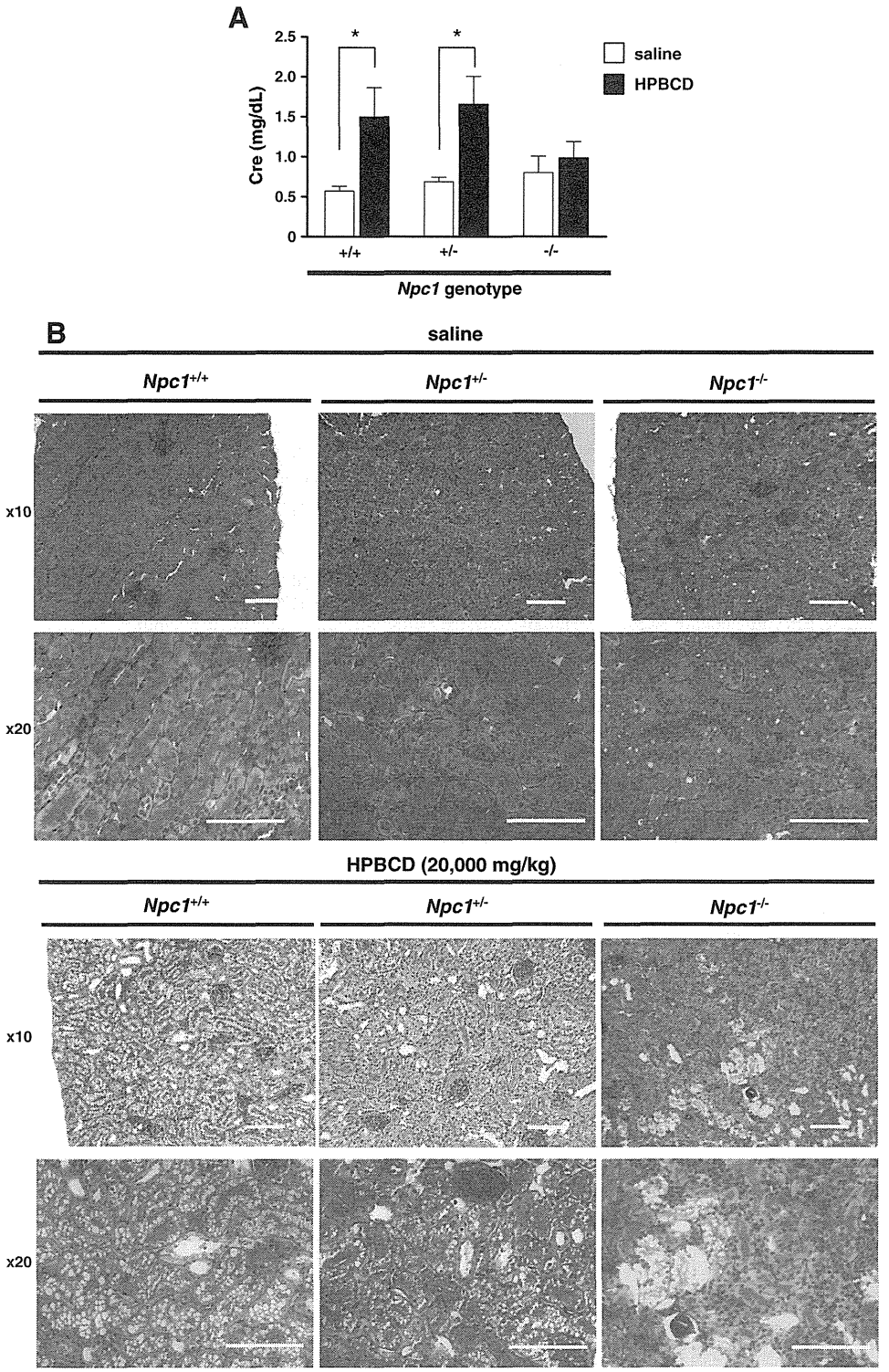
A
Cre (mg/dL)
2.5
2.0
1.5
1.0
0.5
0
*
*
saline
HPBCD
+/+
+/-
-/-
Npc1 genotype
B
saline
Npc1+/+
Npc1+/-
Npc1-/-
x10
x20
HPBCD (20,000 mg/kg)
Npc1+/+
Npc1+/-
Npc1-/-
x10
x20

Meier analysis, significant differences were observed in the *Npc1*$^{-/-}$ group compared with the *Npc1*$^{+/+}$ and *Npc1*$^{+/-}$ groups. Although statistical significances were not observed between the *Npc1*$^{+/+}$ and *Npc1*$^{+/-}$ groups, the survival of the *Npc1*$^{+/+}$ group tended to be lower than that of the *Npc1*$^{+/-}$ groups ($p = 0.108$ in log-rank test).

3.2. Biochemical and histological analysis of Npc1 mutant mice treated with a toxic dose of HPBCD

3.2.1. Liver

The measurements of serum ALT levels and histological analysis were performed 8 h after subcutaneous administration of HPBCD (20,000 mg/kg) in the *Npc1*$^{+/+}$ or *Npc1* mutant mice. As shown in Fig. 2A, serum ALT levels were significantly increased in the HPBCD-treated groups compared with the saline-treated groups of both *Npc1*$^{+/+}$ and *Npc1*$^{+/-}$ mice. Although significant differences were not observed between saline- and HPBCD-treated groups in *Npc1*$^{-/-}$ mice, the *Npc1*$^{-/-}$ mice showed high serum ALT levels (approximately 1000 IU/L) in both the saline- and HPBCD-treated groups. The histological section of the HPBCD-treated *Npc1*$^{+/+}$ and *Npc1*$^{+/-}$ mice showed extensive hepatocellular necrosis with congestion and infiltration of inflammatory cells, such as lymphocytes. In contrast, these pathological changes were not observed in the saline-treated *Npc1*$^{+/+}$ and *Npc1*$^{+/-}$ mice (Fig. 2B). Many vacuolated hepatocytes and Kupffer cells in the histological section and hepatomegaly and fatty liver-like morphology were observed in both the saline- and HPBCD-treated groups in *Npc1*$^{-/-}$ mice. However, hepatocellular necrosis as shown in the HPBCD-treated *Npc1*$^{+/+}$ and *Npc1*$^{+/-}$ mice was not observed in *Npc1*$^{-/-}$ mouse groups.

3.2.2. Kidney

To evaluate renal toxicity, measurements of serum creatinine concentration and histological analysis were performed 8 h after subcutaneous administration of HPBCD (20,000 mg/kg) in *Npc1* mutant mice. As shown in Fig. 3A, serum creatinine levels were significantly increased in the HPBCD-treated groups compared with the saline-treated groups of both *Npc1*$^{+/+}$ and *Npc1*$^{+/-}$ mice. In contrast, little difference in the serum creatinine level was observed between the saline- and HPBCD-treated groups in *Npc1*$^{-/-}$ mice. Although urinary hemorrhage was observed in the HPBCD-treated *Npc1*$^{+/+}$ and *Npc1*$^{+/-}$ mouse groups, no changes were observed in the HPBCD-treated *Npc1*$^{-/-}$ group. In histological analysis, significant vacuolization of the tubular epithelium and hyperplasia of the Bowman capsule were observed in the HPBCD-treated *Npc1*$^{+/+}$ and *Npc1*$^{+/-}$ mouse groups (Fig. 3B). However, a slight degree of histological change induced by HPBCD was observed in the *Npc1*$^{-/-}$ mouse groups.

3.2.3. Lung

Lung histological sections of the saline-treated *Npc1*$^{+/+}$ and *Npc1*$^{+/-}$ mouse groups exhibited normal morphology. In contrast, severe hemorrhage, infiltration of inflammatory cells, and thickened alveolar septum were observed in the HPBCD-treated *Npc1*$^{+/+}$ and *Npc1*$^{+/-}$ mouse groups (Fig. 4A). Many vacuolated alveolar macrophages were found in both the saline- and HPBCD-treated *Npc1*$^{-/-}$ mouse groups. Minor lung pathological changes that were exhibited in the HPBCD-treated *Npc1*$^{+/+}$ and *Npc1*$^{+/-}$ mouse groups were also observed in the HPBCD-treated *Npc1*$^{-/-}$ mouse group. As shown in Fig. 4B, the histopathological scores in the HPBCD-treated groups were significantly higher than in the saline-treated *Npc1*$^{+/+}$ and *Npc1*$^{+/-}$ mouse groups. In contrast, significant differences were not observed between the HPBCD- and saline-treated groups of *Npc1*$^{-/-}$ mice.

3.3. In vitro analysis of HPBCD-induced cell injury

As shown in Fig. 5A, treatment with HPBCD induced a decrease in cell viability in wild-type CHO cells in a dose-dependent manner. Significant decreases were observed when cells were treated with 30 mM or higher HPBCD. In *Npc1* null CHO cells, statistically significant decreases in cell viability were observed

Fig. 3. Renal biochemical and histological analysis of wild-type and *Npc1* mutant mice treated with a toxic dose of HPBCD. Serum creatinine levels (A) and representative renal sections (periodic acid-Schiff stained) (B) 8 h after saline or HPBCD (20,000 mg/kg) subcutaneous injection. Values are the mean ± S.E.M., ($n = 5$–7). * $P < 0.05$; n.s., not significant. Scale bar = 400 μm.

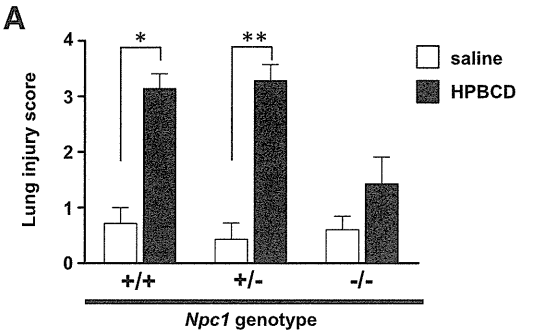
A
Lung injury score
0
1
2
3
4
*
**
saline
HPBCD
+/+
+/-
-/-
Npc1 genotype

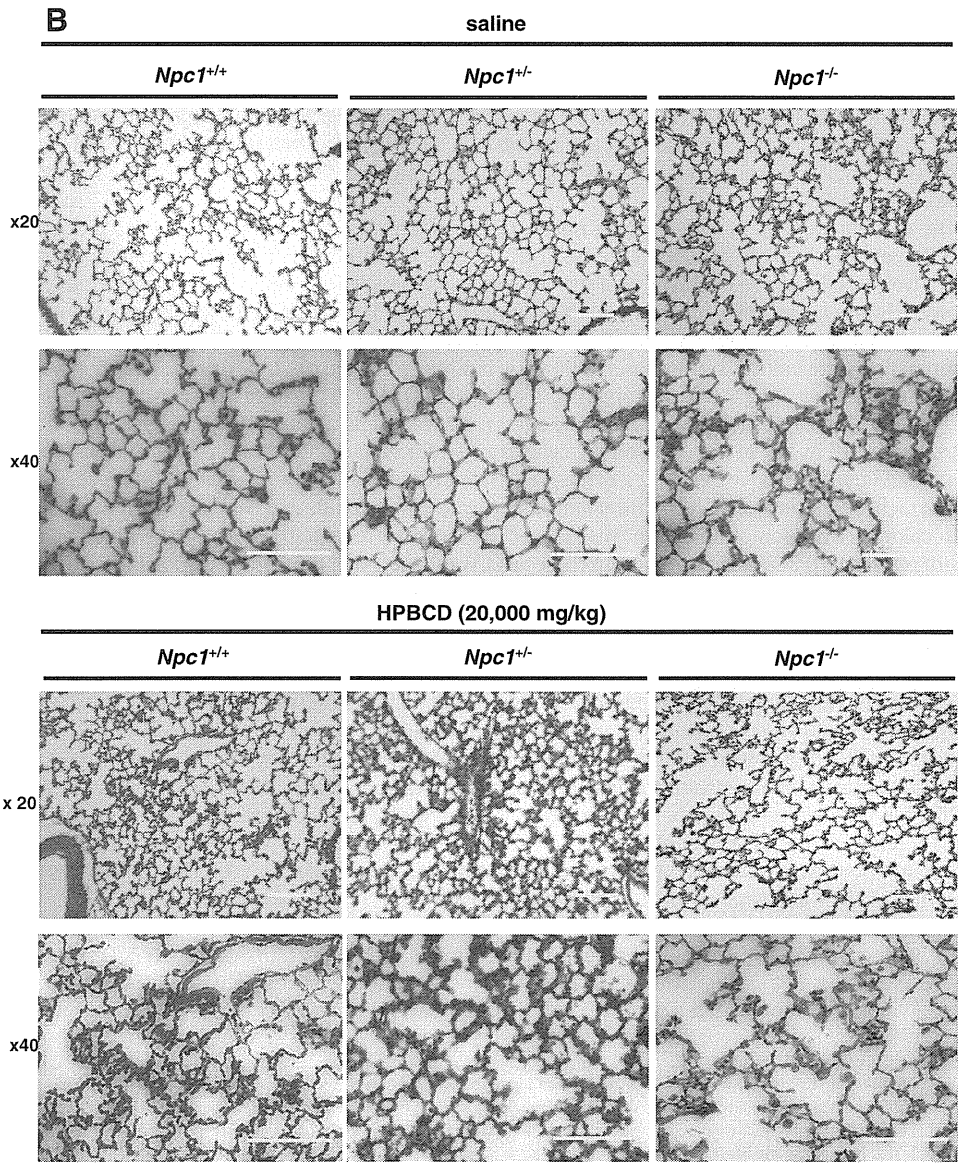
B
saline
Npc1+/+
Npc1+/-
Npc1-/-
x20
x40
HPBCD (20,000 mg/kg)
Npc1+/+
Npc1+/-
Npc1-/-
x 20
x40

when cells were treated with 60 mM or higher HPBCD. There were significant differences in the decrease in cell viability induced by HPBCD between wild-type and *Npc1* null cells. Representative fluorescence images of calcein-AM and PI co-stained cells are shown in Fig. 5B. Although a significant number of PI-stained cells (red) were observed when wild-type cells were treated with HPBCD, many cells were stained with calcein-AM (green) in *Npc1* null cells after HPBCD treatment. In addition, the decreases in cell viability induced by HPBCD (60–80 mM) exposure were significantly attenuated by pretreatment with U18666A (1 μM), an Npc1 inhibitor, in wild-type CHO cells (Fig. 5C). The increase in PI-stained cells (red) and decrease in calcein-AM-stained cells (green) induced by HPBCD exposure in wild-type cells were reduced by treatment with U18666A (Fig. 5D).

4. Discussion

In this study, we demonstrated that a subcutaneous injection of 20,000 mg/kg HPBCD induced over 50% death within 72 h and severe injury of principal organs, such as the liver, kidneys, and lungs, at 8 h after injection in $Npc1^{+/+}$ and $Npc1^{+/-}$ mice. In contrast, we demonstrated that the lethality and organ injury attributed to an injection of HPBCD were alleviated in $Npc1^{-/-}$ mice. These results suggest that $Npc1^{-/-}$ mice have substantial resistance to the lethality and organ injury induced by HPBCD injection compared with $Npc1^{+/+}$ and $Npc1^{+/-}$ mice. In addition, the *in vitro* data demonstrated that HPBCD-induced cell injury was mild in *Npc1* null cells compared with wild-type cells and suggests that the *Npc1* genotype influences the cytotoxicity of HPBCD.

The data on survival in *Npc1* mutant mice suggest that a subcutaneous injection of 20,000 mg/kg of HPBCD may approximate a sublethal dose (50% to 80% lethal doses) in $Npc1^{+/+}$ and $Npc1^{+/-}$ mice, respectively. Although the exact cause of the lethality is unknown, acute multiple organ injury seems to be involved. Severe hepatocellular necrosis with accumulation of inflammatory cells, significant vacuolization of the renal tubular epithelium, an increase in serum creatinine level, severe pulmonary hemorrhage, and inflammation were induced by this dose of HPBCD in both $Npc1^{+/+}$ and $Npc1^{+/-}$ mice at 8 h after injection. In contrast, less lethality and less severe organ injuries by HPBCD in $Npc1^{-/-}$ mice compared with $Npc1^{+/+}$ and $Npc1^{+/-}$ mice indicate that the *Npc1* genotype affects cell death sensitivity of HPBCD in mice. This suggestion is also supported by our *in vitro* data on the cytotoxicity induced by HPBCD in wild-type and *Npc1* null CHO cells. In addition, Appelqvist et al. [13,14] demonstrated that the *NPC1* mutant and U18666A-treated cells show a higher resistance to cellular injury induced by hydrogen peroxide and O-methyl-serine dodecylamide hydrochloride, a lysosomotropic apoptosis inducer. Their reports seem to be concordant with our *in vivo* and *in vitro* results of HPBCD toxicity. Based on these facts, we suggest that the *Npc1* mutation plays an important role in cellular/organ injury induced by high doses of HPBCD.

The results of our present study may be valuable to evaluate the safety of HPBCD therapy for patients with NPC disease. Thus far, HPBCD is the only attractive drug candidate to treat NPC disease and offers a small ray of hope for an effective cure for these patients. However, some reports strike a note of warning for the use of HPBCD in NPC patients [7–9]. Chien et al. [7] showed the possibility of HPBCD-induced pneumonia in young pigs and advocated that the pulmonary toxicity of HPBCD should not be neglected. However, the *Npc1* genotype (or function) was not considered in their study. In the present study, we also observed lung injury induced with an injection of a sublethal dose of HPBCD. Additionally, the susceptibility to HPBCD was different between $Npc1^{+/+}$ and $Npc1^{+/-}$, and $Npc1^{-/-}$ mice. Muralidhar et al. [15] and Ramirez et al. [4] reported that treatment of $Npc1^{-/-}$ mice with HPBCD had little or no effect on the development of progressive pulmonary disease. Therefore, when evaluating the safety of HPBCD therapy for NPC disease, the difference of *NPC1* genotype should be considered.

Significantly elevated ALT, hepatomegaly, and fatty liver-like morphology are a recognized hepatic $Npc1^{-/-}$ phenotype [16]. This phenotype seems to obfuscate the hepatotoxicity of HPBCD treatment. In the present study, both saline- and HPBCD-treated $Npc1^{-/-}$ mouse groups as well as the HPBCD-treated $Npc1^{+/-}$ mouse group exhibited high ALT levels. Significant hepatocellular necrosis was not observed in

Fig. 4. Pulmonary histological analysis of wild-type and *Npc1* mutant mice treated with a toxic dose of HPBCD. Representative lung sections (hematoxylin eosin stained) (A) and lung injury scores (B) 8 h after saline or HPBCD (20,000 mg/kg) subcutaneous injection. Lung injury score was measured as described in the Material and Methods. Values are the mean ± S.E.M., (n = 5–7). * $P < 0.05$, ** $P < 0.01$; n.s., not significant. Scale bar = 400 μm.

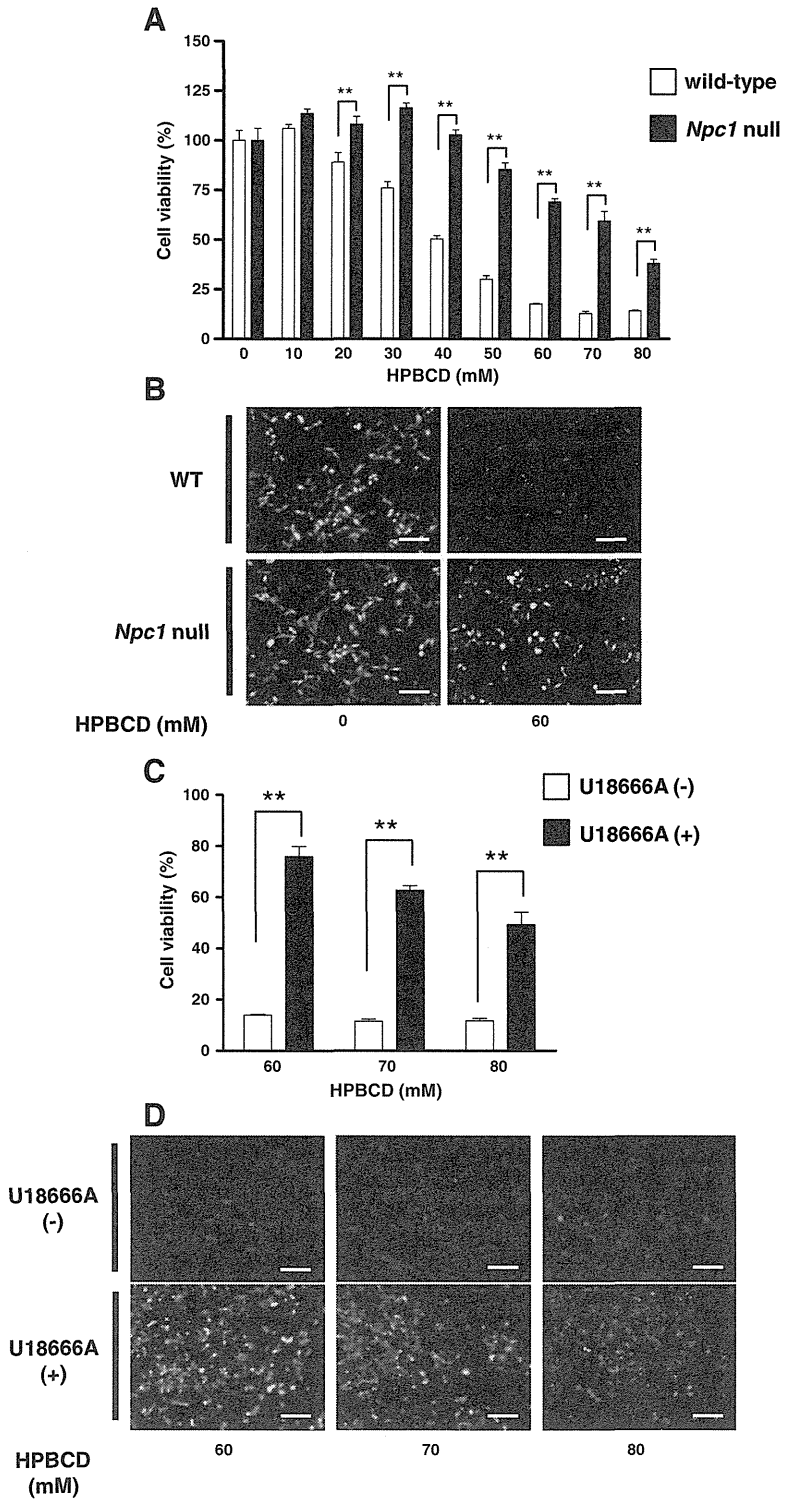
A
Cell viability (%)
150
125
100
75
50
25
0
0 10 20 30 40 50 60 70 80
HPBCD (mM)
wild-type
Npc1 null
**
B
WT
Npc1 null
HPBCD (mM)
0
60
C
Cell viability (%)
100
80
60
40
20
0
60 70 80
HPBCD (mM)
U18666A (-)
U18666A (+)
**
D
U18666A (-)
U18666A (+)
HPBCD (mM)
60
70
80

the HPBCD-treated *Npc1*$^{-/-}$ mouse group compared with the HPBCD-treated *Npc1*$^{+/-}$ mouse group. We considered that the HPBCD-induced hepatotoxicity was not exerted in *Npc1*$^{-/-}$ mice compared with *Npc1*$^{+/-}$ mice.

Although we demonstrated the high tolerability of *Npc1* null CHO cells against HPBCD toxicity compared with wild-type CHO cells, the precise mechanisms of the tolerability are unclear. In our previous study, we demonstrated that there was a positive correlation between *in vitro* hemolytic activity and cholesterol-solubilizing activity of cyclodextrin derivatives and therefore suggested that the cellular injury induced by cyclodextrins was involved in cholesterol extraction from the cell surface membrane [17,18]. Some reports have indicated that *Npc1* null cells or U18666A-treated cells showed a lower cholesterol content in the plasma membrane and a higher content in the lysosome compared with the plasma membrane of non-treated wild-type cells [19–21]. Therefore, we considered that the lower cholesterol portion on the plasma membrane in *Npc1* null cells or U18666A-treated cells may be related to lower toxicity by HPBCD. In addition, Appelqvist et al. demonstrated that *Npc1* null cells or U18666A-treated cells significantly attenuated cell injury induced by O-methyl-serine dodecylamide hydrochloride, an apoptosis inducer, and hydrogen peroxide, an oxidative stress inducer, and suggested that the *Npc1* mutation and inhibition can modulate lysosomal function through an increase in cholesterol content in the lysosome and thereby influence cell death sensitivity [14]. Therefore, complicated mechanisms of tolerability of the *Npc1*-deficient cells against cellular injury seem to be involved. To clarify the precise molecular mechanisms of tolerability to HPBCD toxicity, further study will be necessary.

Although we provided evidence of low susceptibility to acute HPBCD toxicity in *Npc1*$^{-/-}$ mice and CHO cells, further basic and clinical studies are warranted to establish the safety of HPBCD therapy for NPC patients. We examined the acute toxicity of a single high-dose HPBCD treatment in mice in this study. Some previous reports have demonstrated that the usual dosage of HPBCD, which can attenuate cholesterol sequestration in organs and prolong lifespan in *Npc1*$^{-/-}$ mice, was 4000 mg/kg, and it was subcutaneously injected once a week for life [2–4]. Therefore, data of "sub-acute or chronic" safety of "multiple administration" of HPBCD in *Npc1*$^{-/-}$ mice are needed. In addition, information regarding appropriate dosage regimen and blood concentrations of HPBCD, which ensure both efficacy and safety in *Npc1*$^{-/-}$ mice and NPC patients, is insufficient. Therefore, both pharmacokinetic and pharmacodynamic studies of HPBCD in *Npc1*$^{-/-}$ mice and NPC patients are warranted.

In our previous study, NPC patients were administered HPBCD (2000–2500 mg/kg) infusions twice or more per week [5]. Despite administration of high- and multiple-doses of HPBCD, severe adverse reactions were not observed during the therapy periods. In contrast, fever and transient diffuse pulmonary cloudiness on chest X-ray following HPBCD infusion were observed in an NPC patient at 23 months after the start of the HPBCD therapy [5]. The patient also suffered from aspiration pneumonia when the episode of fever and pulmonary cloudiness was observed. Since then, same symptoms have not been observed; however, the possibility of an adverse reaction of HPBCD cannot be denied. Therefore, we considered that further clinical studies are warranted to establish the long-term safety of HPBCD therapy for NPC patients.

5. Conclusion

We demonstrated that the lethality and organ injury induced by an injection of HPBCD, which was observed in *Npc1*$^{+/-}$ mice, were attenuated in *Npc1*$^{-/-}$ mice. In addition, HPBCD-induced cell injury was alleviated in *Npc1* null CHO cells, and the cell injury was also attenuated by U18666A, an Npc1 inhibitor, in wild-type CHO cells. These results suggest that the *Npc1* genotype affects the cytotoxicity of HPBCD, and therefore, *Npc1*$^{-/-}$ mice have substantial resistance to the lethality and organ injury induced by HPBCD injection compared with *Npc1*$^{+/-}$ mice. Up to the present, healthy (wild-type) animals have been used to evaluate the safety of HPBCD as a therapeutic agent for NPC disease. We suggest that the *Npc1* genotype should be considered when performing a safety evaluation of HPBCD therapy for NPC disease in animal or cellular experiments.

Fig. 5. Effect of gene deletion or pharmacological inhibition of NPC1 against HPBCD cytotoxicity. Cell viability was measured 3 h after HPBCD treatment using the WST-8 assay (A and C) and calcein-AM and PI co-staining (B and D). HPBCD-induced cytotoxicity in wild-type or *Npc1* null CHO cells (A and B) and U18666A (1 μM) pretreated CHO cells (C and D). Values are the mean ± S.E.M., (n = 3–4). ** $P < 0.01$; * $P < 0.05$. Scale bar = 100 μm.

Competing interests

The authors declare that they have no competing interests. This work was supported by JSPS KAKENHI Grant Number 23590642.

Acknowledgments

We are grateful to Yuka Horikoshi, Shiori Takeuji, Yumiko Hirose, Koki Shiraishi, Makiko Taguchi and all of the staff of division of reproductive engineering, center for animal resources and development (CARD), Kumamoto University for breeding mice. We also gratefully acknowledge the financial support from the Japan Society for the Promotion of Science (JSPS KAKENHI Grant Number 23590642).

References

[1] M.T. Vanier, Niemann-Pick disease type C, Orphanet J. Rare Dis. 5 (2010) 16.
[2] B. Liu, S.D. Turley, D.K. Burns, A.M. Miller, J.J. Repa, J.M. Dietschy, Reversal of defective lysosomal transport in NPC disease ameliorates liver dysfunction and neurodegeneration in the npc1−/− mouse, Proc. Natl. Acad. Sci. U. S. A. 106 (2009) 2377–2382.
[3] C.D. Davidson, N.F. Ali, M.C. Micsenyi, G. Stephney, S. Renault, K. Dobrenis, D.S. Ory, M.T. Vanier, S.U. Walkley, Chronic cyclodextrin treatment of murine Niemann-Pick C disease ameliorates neuronal cholesterol and glycosphingolipid storage and disease progression, PLoS One 4 (2009) e6951.
[4] C.M. Ramirez, B. Liu, A.M. Taylor, J.J. Repa, D.K. Burns, A.G. Weinberg, S.D. Turley, J.M. Dietschy, Weekly cyclodextrin administration normalizes cholesterol metabolism in nearly every organ of the Niemann-Pick type C1 mouse and markedly prolongs life, Pediatr. Res. 68 (2010) 309–315.
[5] M. Matsuo, M. Togawa, K. Hirabaru, S. Mochinaga, A. Narita, M. Adachi, M. Egashira, T. Irie, K. Ohno, Effects of cyclodextrin in two patients with Niemann-Pick Type C disease, Mol. Genet. Metab. 108 (2013) 76–81.
[6] M.E. Brewster, T. Loftsson, Cyclodextrins as pharmaceutical solubilizers, Adv. Drug Deliv. Rev. 59 (2007) 645–666.
[7] Y.H. Chien, Y.D. Shieh, C.Y. Yang, N.C. Lee, W.L. Hwu, Lung toxicity of hydroxypropyl-beta-cyclodextrin infusion, Mol. Genet. Metab. 109 (2013) 231–232.
[8] E.A. Thackaberry, S. Kopytek, P. Sherratt, K. Trouba, B. McIntyre, Comprehensive investigation of hydroxypropyl methylcellulose, propylene glycol, polysorbate 80, and hydroxypropyl-beta-cyclodextrin for use in general toxicology studies, Toxicol. Sci. 117 (2010) 485–492.
[9] M.L. Rosseels, A.G. Delaunois, E. Hanon, P.J. Guillaume, F.D. Martin, D.J. van den Dobbelsteen, Hydroxypropyl-beta-cyclodextrin impacts renal and systemic hemodynamics in the anesthetized dog, Regul. Toxicol. Pharmacol. 67 (2013) 351–359.
[10] S.K. Loftus, Murine model of Niemann-Pick C disease: mutation in a cholesterol homeostasis gene, Science 277 (1997) 232–235.
[11] S. Furue, K. Kuwabara, K. Mikawa, K. Nishina, M. Shiga, N. Maekawa, M. Ueno, Y. Chikazawa, T. Ono, Y. Hori, A. Matsukawa, M. Yoshinaga, H. Obara, Crucial role of group IIA phospholipase A(2) in oleic acid-induced acute lung injury in rabbits, Am. J. Respir. Crit. Care Med. 160 (1999) 1292–1302.
[12] K. Higaki, H. Ninomiya, Y. Sugimoto, T. Suzuki, M. Taniguchi, H. Niwa, P.G. Pentchev, M.T. Vanier, K. Ohno, Isolation of NPC1-deficient Chinese hamster ovary cell mutants by gene trap mutagenesis, J. Biochem. 129 (2001) 875–880.
[13] H. Appelqvist, C. Nilsson, B. Garner, A.J. Brown, K. Kagedal, K. Ollinger, Attenuation of the lysosomal death pathway by lysosomal cholesterol accumulation, Am. J. Pathol. 178 (2011) 629–639.
[14] H. Appelqvist, L. Sandin, K. Bjornstrom, P. Saftig, B. Garner, K. Ollinger, K. Kagedal, Sensitivity to lysosome-dependent cell death is directly regulated by lysosomal cholesterol content, PLoS One 7 (2012) e50262.
[15] A. Muralidhar, I.A. Borbon, D.M. Esharif, W. Ke, R. Manacheril, M. Daines, R.P. Erickson, Pulmonary function and pathology in hydroxypropyl-beta-cyclodextin-treated and untreated Npc1(−)/(−) mice, Mol. Genet. Metab. 103 (2011) 142–147.
[16] E.P. Beltroy, J.A. Richardson, J.D. Horton, S.D. Turley, J.M. Dietschy, Cholesterol accumulation and liver cell death in mice with Niemann-Pick type C disease, Hepatology 42 (2005) 886–893.
[17] T. Irie, K. Uekama, Pharmaceutical applications of cyclodextrins. III. Toxicological issues and safety evaluation, J. Pharm. Sci. 86 (1997) 147–162.
[18] K.M. Wojtanik, L. Liscum, The transport of low density lipoprotein-derived cholesterol to the plasma membrane is defective in NPC1 cells, J. Biol. Chem. 278 (2003) 14850–14856.
[19] E.P. Kilsdonk, P.G. Yancey, G.W. Stoudt, F.W. Bangerter, W.J. Johnson, M.C. Phillips, G.H. Rothblat, Cellular cholesterol efflux mediated by cyclodextrins, J. Biol. Chem. 270 (1995) 17250–17256.
[20] Y. Lange, J. Ye, M. Rigney, T. Steck, Cholesterol movement in Niemann-Pick type C cells and in cells treated with amphiphiles, J. Biol. Chem. 275 (2000) 17468–17475.
[21] Y. Tashiro, T. Yamazaki, Y. Shimada, Y. Ohno-Iwashita, K. Okamoto, Axon-dominant localization of cell-surface cholesterol in cultured hippocampal neurons and its disappearance in Niemann-Pick type C model cells, Eur. J. Neurosci. 20 (2004) 2015–2021.

Cell Stem Cell
Article

Human iPSC-Based Modeling of Late-Onset Disease via Progerin-Induced Aging

Justine D. Miller,[1,2,3] Yosif M. Ganat,[1,2] Sarah Kishinevsky,[1,2] Robert L. Bowman,[3,4] Becky Liu,[1,2] Edmund Y. Tu,[1,2] Pankaj K. Mandal,[6,7] Elsa Vera,[1,2] Jae-won Shim,[1,2] Sonja Kriks,[1,2] Tony Taldone,[5] Noemi Fusaki,[8,9] Mark J. Tomishima,[1,2] Dimitri Krainc,[10] Teresa A. Milner,[11,12] Derrick J. Rossi,[6,7] and Lorenz Studer[1,2,*]

[1]The Center for Stem Cell Biology, Sloan-Kettering Institute for Cancer Research, 1275 York Avenue, New York, NY 10065, USA
[2]Developmental Biology Program, Sloan-Kettering Institute for Cancer Research, 1275 York Avenue, New York, NY 10065, USA
[3]Gerstner Sloan-Kettering Graduate School, Sloan-Kettering Institute for Cancer Research, 1275 York Avenue, New York, NY 10065, USA
[4]Cancer Biology and Genetics Program, Sloan-Kettering Institute for Cancer Research, 1275 York Avenue, New York, NY 10065, USA
[5]Molecular Pharmacology & Chemistry, Sloan-Kettering Institute for Cancer Research, 1275 York Avenue, New York, NY 10065, USA
[6]Program in Cellular and Molecular Medicine, Boston Children's Hospital, Boston, MA 02115, USA
[7]Department of Stem Cell and Regenerative Biology, Harvard University, Cambridge, MA 02138, USA
[8]DNAVEC Corporation, Tsukuba, Ibaraki 300-2611, Japan
[9]Department of Ophthalmology, Keio University School of Medicine, 35 Shinanomachi, Shinjuku-ku, Tokyo 1608582, Japan
[10]Department of Neurology, Massachusetts General Hospital, Harvard Medical School, Massachusetts General Institute for Neurodegenerative Disease, Charlestown, MA 02129, USA
[11]Brain and Mind Research Institute, Weill Cornell Medical College, 407 East 61st Street, New York, NY 10065, USA
[12]Harold and Margaret Milliken Hatch Laboratory of Neuroendocrinology, The Rockefeller University, 1230 York Avenue, New York, NY 10065, USA
*Correspondence: studerl@mskcc.org
http://dx.doi.org/10.1016/j.stem.2013.11.006

SUMMARY

Reprogramming somatic cells to induced pluripotent stem cells (iPSCs) resets their identity back to an embryonic age and, thus, presents a significant hurdle for modeling late-onset disorders. In this study, we describe a strategy for inducing aging-related features in human iPSC-derived lineages and apply it to the modeling of Parkinson's disease (PD). Our approach involves expression of progerin, a truncated form of lamin A associated with premature aging. We found that expression of progerin in iPSC-derived fibroblasts and neurons induces multiple aging-related markers and characteristics, including dopamine-specific phenotypes such as neuromelanin accumulation. Induced aging in PD iPSC-derived dopamine neurons revealed disease phenotypes that require both aging and genetic susceptibility, such as pronounced dendrite degeneration, progressive loss of tyrosine hydroxylase (TH) expression, and enlarged mitochondria or Lewy-body-precursor inclusions. Thus, our study suggests that progerin-induced aging can be used to reveal late-onset age-related disease features in hiPSC-based disease models.

INTRODUCTION

Late-onset neurodegenerative disorders such as Parkinson's disease (PD) are becoming a growing burden to society due to the gradual increase in life expectancy. The incidence of PD will likely continue to rise because it is estimated that by 2050, 21.8% of the projected world population (approximately two billion people) will be over 60 years of age (Lutz et al., 2008). The use of induced pluripotent stem cell (iPSC) technology where patient-derived skin cells can be reprogrammed back to a pluripotent state and then further differentiated into disease-relevant cell types presents new opportunities for modeling and potentially treating currently intractable human disorders (Bellin et al., 2012). However, there is a concern as to how well iPSC-derived cells can model late-onset diseases where patients do not develop symptoms until later in life, implicating age as a necessary component to disease progression. Several iPSC studies have demonstrated a loss of particular age-associated features during iPSC induction (reviewed in Freije and López-Otín, 2012; Mahmoudi and Brunet, 2012). For instance, there is evidence for an increase in telomere length (Agarwal et al., 2010; Marion et al., 2009) and mitochondrial fitness (Prigione et al., 2010; Suhr et al., 2010) and loss of senescence markers (Lapasset et al., 2011) in iPSCs derived from old donors, suggesting that rejuvenation takes place during reprogramming. In addition to the apparent loss of age-associated features in iPSCs, the directed differentiation of human pluripotent stem cells (hPSCs) is known to yield immature, embryonic-like cell types that often require months of maturation to establish robust functional properties (Liu et al., 2012a; Saha and Jaenisch, 2009). Protracted differentiation is thought to reflect the slow timing of human development. For example, human midbrain dopamine (mDA) neurons, a cell type affected in PD, require months of differentiation to develop mature physiological behaviors and to rescue dopamine deficits in animal models of PD (Isacson and Deacon, 1997; Kriks et al., 2011). These in vitro differentiation data argue for a species-specific, intrinsic "clock-like" mechanism that prevents the rapid generation of mature, and aged, cells posing a challenge for human iPSC-based modeling of late-onset disorders.

A key problem in addressing global aspects of aging and rejuvenation during cell reprogramming is the identification of

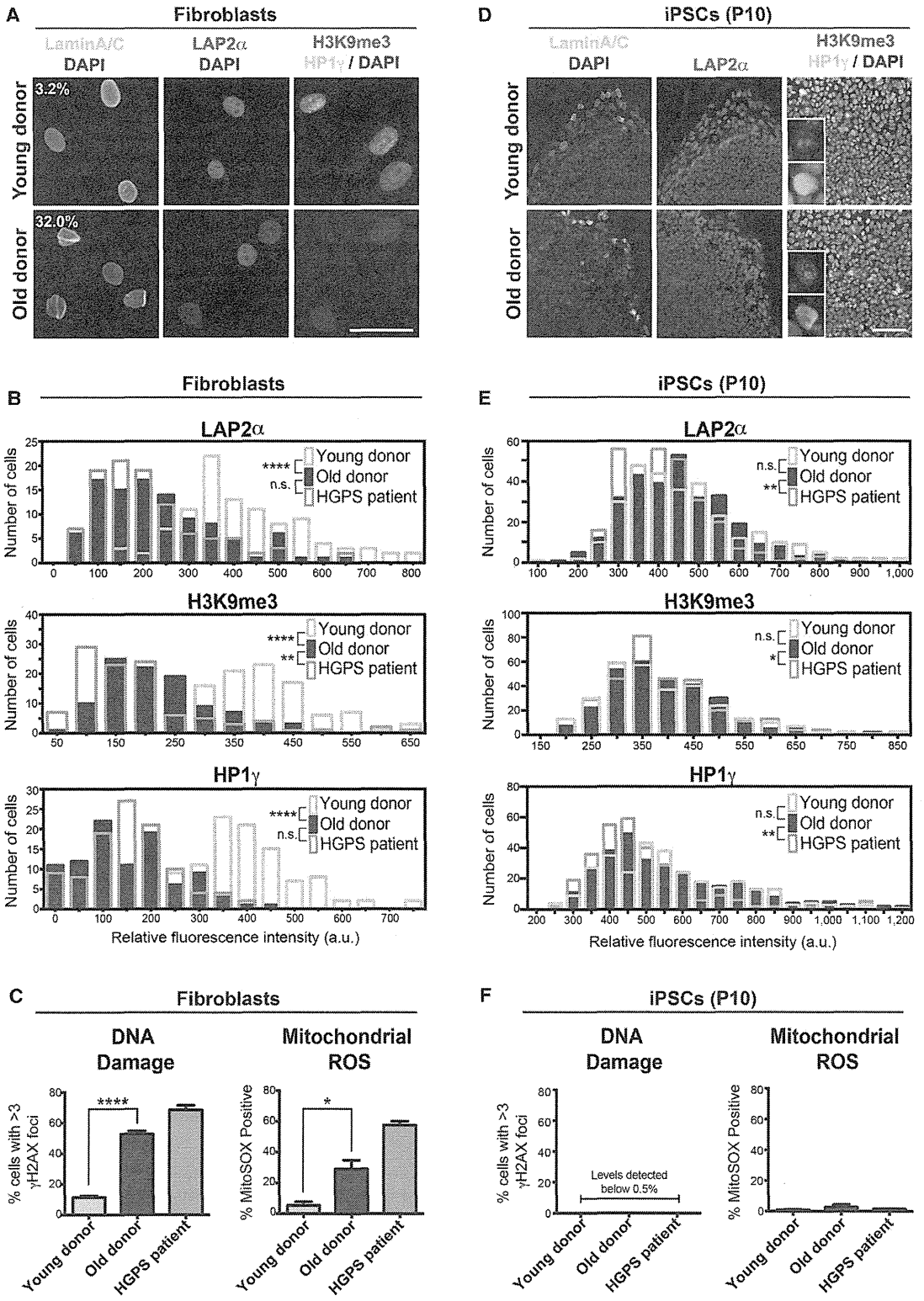

Figure 1. Old Donor Fibroblasts Lose Age-Associated Markers following Reprogramming to the Pluripotent State

(A) Immunocytochemistry shows markers identifying the nuclear lamina (lamin A/C), a lamina-associated protein (LAP2α), and peripheral heterochromatin (H3K9me3 and HP1γ) in young fibroblasts (11-year-old donor) compared to old fibroblasts (82-year-old donor). Percentages indicate the proportion of cells with folded and/or blebbed nuclear morphologies.

(legend continued on next page)

markers that reliably measure age in vitro. Candidate age-related cellular markers have been described in fibroblasts derived from patients with Hutchinson-Gilford progeria syndrome (HGPS) (Scaffidi and Misteli, 2005, 2006). HGPS is a rare genetic disorder characterized by premature aging of various tissues resulting in early death (Hennekam, 2006). Mutations in *LMNA*, the gene coding for the nuclear envelope protein lamin A, result in the activation of a cryptic splice site that produces a shorter transcript known as progerin. Progerin protein aberrantly accumulates in the nuclear membrane, preventing at least some of the normal scaffolding functions of lamin A, which in turn interferes with multiple processes in the nucleus, including chromatin organization, heterochromatin formation, the DNA-damage response, cell cycle, gene transcription, and telomere maintenance (reviewed in Dechat et al., 2008). Interestingly, low levels of progerin are expressed in healthy individuals, and a similar age-associated profile has been observed in fibroblasts from normally aged donors (Scaffidi and Misteli, 2006).

Here, we utilize a set of markers that correlates with fibroblast donor age, including markers of nuclear morphology and expression of nuclear organization proteins as well as markers of heterochromatin, DNA damage, and reactive oxygen species (ROS). Such age-associated markers, present in old fibroblasts, were lost during reprogramming and were not reacquired during the subsequent differentiation, indicating that iPSC-derived cells do not maintain a memory of their age. Importantly, we could induce tissue-specific age-associated markers in both iPSC-derived fibroblasts (iPSC-fibroblasts) and iPSC-derived mDA neurons (iPSC-mDA neurons) following short-term progerin exposure. The ability to rapidly induce features associated with cellular age was captured to improve modeling PD in vitro and upon transplantation of iPSC-mDA neurons in vivo. We observed several age- and disease-related phenotypes not seen in previous iPSC studies, including evidence of dendrite degeneration, the formation of age-associated neuromelanin, AKT deregulation, reduction in the number of TH^+ neurons, and ultrastructural evidence of mitochondrial swelling and inclusion bodies. Induced aging presents a paradigm for iPSC studies that may be applicable to other cell types and disease pathologies to address the contribution of genetic and age-associated factors in late-onset disorders.

RESULTS

Reprogramming Reverts Age-Associated Markers to a "Young" State

In order to validate a marker profile that could be followed during reprogramming and redifferentiation, we compared 12 passage-matched fibroblast populations from apparently healthy young donors (age 11), middle-aged donors (ages 31–55), old donors (ages 71–96), and prematurely aged patients with HGPS (ages 3–14) (Table S1 available online). We observed a significant correlation of donor fibroblast age with age-associated markers (Figures 1A–1C and S1A), including markers previously described in HGPS fibroblasts (Scaffidi and Misteli, 2006). Fibroblasts from old donors resembled HGPS fibroblasts supporting previous findings by Misteli and colleagues (Scaffidi and Misteli, 2005, 2006). More specifically, old donor fibroblasts showed nuclear morphology abnormalities (i.e., folding and blebbing), loss of the nuclear lamina-associated protein 2α (LAP2α), global loss of the heterochromatin markers trimethylated H3K9 (H3K9me3) and heterochromatin protein 1 γ (HP1γ), as well as an increase in DNA damage and mitochondrial reactive oxygen species (mtROS) levels when compared to fibroblasts from younger donors. Importantly, marker expression in old donor fibroblasts was comparable to HGPS fibroblasts despite expressing low levels of progerin, the mutant protein involved in HGPS (Figure S1B; Table S2). These data suggest that age-associated markers can faithfully stratify young versus old donor fibroblasts.

To address the effects of reprogramming on markers of cellular age, we selected fibroblasts from young (age 11), old (age 82), and HGPS (age 14) donors and transduced them with Sendai vectors expressing Oct4, Sox2, Klf4, and c-Myc (Fusaki et al., 2009) (Figure S1C). The use of the cytoplasmic RNA viruses allowed for the derivation of integration-free iPSCs by 25–40 days posttransduction. All iPSC clones demonstrated pluripotent properties and marker expression (Figures S1D–S1F) and had a normal karyotype (data not shown), and iPSCs derived from HGPS patient fibroblasts maintained the disease mutation (Figure S1G). We next reassessed the age-associated molecular markers shown above to distinguish between young and old fibroblasts. iPSCs were not assessed prior to passage 10 to ensure loss of the exogenous Sendai virus (Figure S1D). Following reprogramming, iPSCs that were derived from old donor fibroblasts were indistinguishable from young donor-derived iPSCs with respect to expression of lamin A, LAP2α, H3K9me, and HP1γ (Figures 1D and 1E). Furthermore, all iPSCs displayed minimal levels of DNA damage or mtROS (Figure 1F), suggesting a reset of phenotypic age. However, the age-associated signature could be dependent on progerin expression (Scaffidi and Misteli, 2006), and the absence of an age-related phenotype in iPSCs may simply reflect the fact that pluripotent cells do not express A-type lamins including progerin (Constantinescu et al., 2006). Immunocytochemical analysis for all A-type lamin isoforms showed expression restricted to cells undergoing

(B) Quantification of the markers depicted in (A) demonstrates the ability of the selected age-associated markers to stratify young versus old donor fibroblasts and the similarity of old donor fibroblasts to HGPS patient fibroblasts. The data are plotted as frequency distributions of relative fluorescence intensity for 100 cells from single fibroblast lines that were passage matched. a.u., arbitrary units.

(C) Similar to HGPS patient fibroblasts, old donor fibroblasts have higher levels of DNA damage (measured by γH2AX immunocytochemistry) and higher levels of mtROS (measured by flow cytometry using the superoxide indicator MitoSOX) than young donor fibroblasts (n = 3 independent experiments).

(D) Immunocytochemistry shows age-associated markers in passage 10 (P10) iPSCs derived from the young and old donor fibroblasts.

(E) Quantification of staining in (D) indicates loss of age-associated markers during reprogramming of old donor-derived iPSCs (similar to HGPS-derived iPSCs). n = 300 cells each (100 cells from three independent iPSC clones).

(F) DNA damage and mtROS levels are reset upon reprogramming (n = 3 independent clones).

n.s., not significant. *$p < 0.05$, **$p < 0.01$, and ****$p < 0.0001$, according to Kolmogorov-Smirnov tests (B and E) or Student's t tests (C and F). Bar graphs represent mean ± SEM. Scale bars, 50 μm (A) and 100 μm (D).

See also Figures S1 and S7, and Tables S1, S2, S4 and S5.

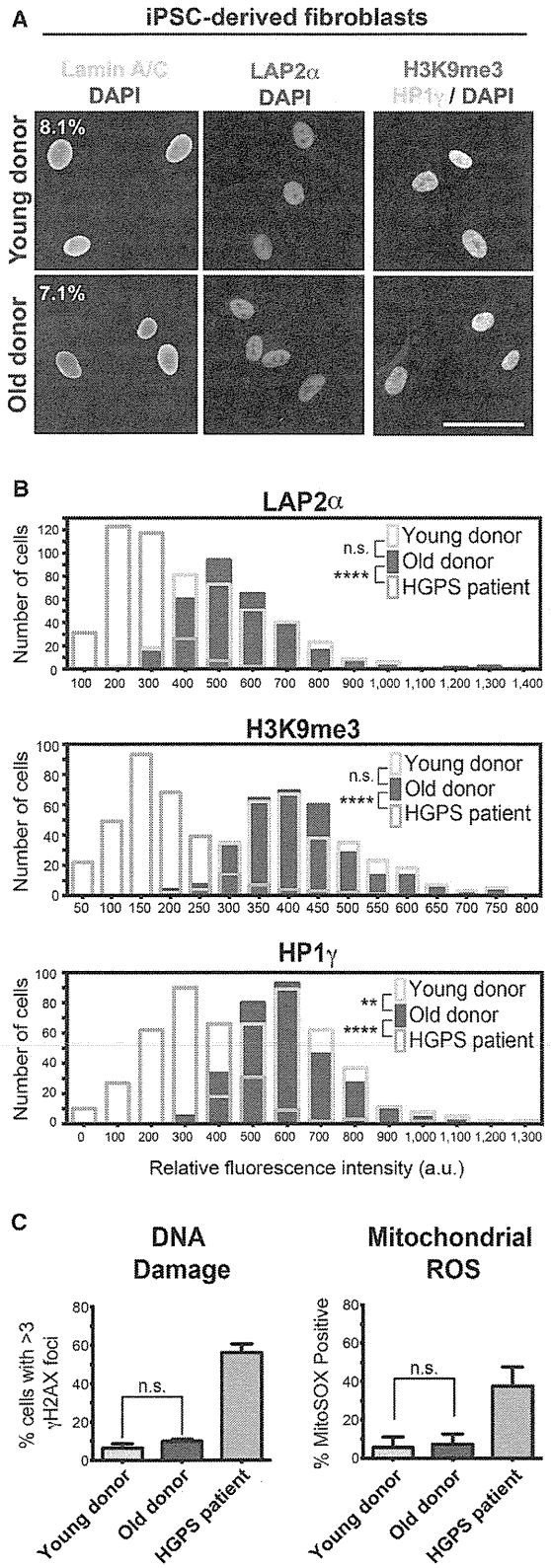

Figure 2. iPSC-Fibroblasts from Old Donors Do Not Regain Age-Associated Markers

(A) Immunocytochemistry for age-associated markers is presented. Percentages indicate the proportion of cells with folded and/or blebbed nuclear morphologies. Scale bar, 50 μm.

(B) Quantification of the markers shown in (A) indicates the high degree of overlap between iPSC-fibroblasts from young and old donors compared to HGPS iPSC-fibroblasts, which reestablish an age-like phenotype.

(C) Analysis of DNA damage (left) and mitochondrial superoxide (right) further shows that iPSC-fibroblasts from old donors have been reset to a "young"-like state.

**$p < 0.01$ and ****$p < 0.0001$, according to Kolmogorov-Smirnov tests (B) or Student's t tests (C). n = 3 differentiations of independent iPSC clones performed at different times. Bar graphs represent mean ± SEM.

See also Figures S2 and S7, and Tables S4 and S5.

spontaneous differentiation at the periphery of iPSC colonies (Figure 1D, left column). HGPS iPSCs demonstrated a comparable loss of age-associated markers at the pluripotent stage, (Figures 1B, 1C, 1E, and 1F). However, despite the loss of age-related markers, our data do not rule out the possibility that reprogramming selects for cells with low levels of age-related marker expression (a "young" cell) among the old donor fibroblasts rather than truly resetting age. Interestingly, clonal growth of primary donor fibroblasts resulted in cultures that reestablished a distribution of age-related markers comparable to the original fibroblast population within 2 weeks (data not shown). Therefore, it was not possible to obtain fibroblast populations homogeneous in the expression of age-related markers. Nevertheless, regardless of the mechanism, our results demonstrate that iPSCs, independent of donor age or HGPS status, lack expression of age-associated markers.

Age Is Not Induced after Differentiating iPSCs Derived from Old Donors

We next tested whether old donor-derived iPSCs may retain a memory of their donor age that is transiently suppressed at the pluripotent stage. We differentiated iPSCs back into fibroblast-like cells using serum-containing medium (Figure S2A) for 30 days followed by fluorescence-activated cell sorting (FACS) for $CD13^{+}/HLA\text{-}ABC^{hi}$ (Papapetrou et al., 2009; Verlinden et al., 1981) (Figure S2B). The purified cells were expanded for an additional 30 days prior to characterization for the fibroblast marker vimentin and absence of the neural precursor marker nestin (Figure S2C). iPSC-fibroblasts showed expression of lamin A and progerin at levels similar to those observed in primary donor fibroblasts (Figure S2D). However, differentiation did not reestablish the age-associated marker profile in old donor iPSC-fibroblasts (Figures 2A–2C) that closely matched the profile of passage-matched young donor iPSC-fibroblasts. These data demonstrate that age-associated markers in primary fibroblasts from aged, apparently healthy donors are reset following reprogramming and are not reestablished upon differentiation into iPSC-fibroblasts. Thus, age is lost after reprogramming, giving rise to phenotypically young iPSC-fibroblasts that may require years of in vitro culture to reestablish their age. In contrast, HGPS iPSC-fibroblasts did spontaneously reestablish expression of age-associated markers upon differentiation (Figures 2B and 2C) as reported in iPSC-based models of HGPS (Liu et al., 2011; Zhang et al., 2011), suggesting that cues such as

high levels of progerin expression can return iPSC-fibroblasts to an aged-like state.

Acute Progerin Overexpression Reestablishes Age-Related Markers in iPSC-Fibroblasts

We next sought to determine whether progerin overexpression is sufficient to induce age-associated markers in apparently healthy young or old donor iPSC-fibroblasts. Synthetic mRNA (termed modified-RNA) (Karikó et al., 2005; Warren et al., 2010) was used to overexpress either GFP fused to progerin (GFP-progerin) or a nuclear-localized GFP control (nuclear-GFP; Figure S2E; Table S2), allowing for easy manipulation of the amount and duration of expression. Daily transfection of modified-RNA for 3 days (Figure 3A) induced progerin expression to levels similar or higher than those in HGPS iPSC-fibroblasts (Figure S2F, arrows). Strikingly, overexpression of GFP-progerin but not nuclear-GFP in young and old donor iPSC-fibroblasts induced nuclear morphology abnormalities, loss of LAP2α expression, formation of DNA double-strand breaks (γH2AX), loss of heterochromatin markers (H3K9me3 and HP1γ), and increased mtROS (Figures 3B–3D). These progerin-induced features were indistinguishable from those observed in primary fibroblasts from aged donors (Figures 1A–1C and S1A). Aging in mitotic cells is typically associated with the shortening of telomeres to a critical point when the cell undergoes senescence, reaching Hayflick's limit (Hayflick, 1965). Therefore, we measured telomere lengths using quantitative fluorescence in situ hybridization (Canela et al., 2007) in transfected iPSC-fibroblasts to determine whether progerin can induce telomere shortening. Following progerin overexpression, iPSC-fibroblasts demonstrated a decrease in overall length and an increase in the percentage of short telomeres with progerin overexpression (Figure S2G). This result was further corroborated by an increase in senescence-activated β-galactosidase (SA-β-gal) staining (Figure S2H). All progerin-induced changes in iPSC-fibroblasts were independent of donor age. Our observations indicate that progerin overexpression is sufficient to rapidly induce phenotypes in iPSC-fibroblasts that phenocopy aspects of normal aging.

Progerin Induces Neuronal Aging Phenotypes in iPSC-mDA Neurons

We next tested whether progerin overexpression also induces age-like phenotypes in a postmitotic cell type. Therefore, we differentiated young and old donor iPSCs into mDA neurons, a cell type affected in PD, using our previously established protocol (Kriks et al., 2011) (Figure S3A). Within 13 days, differentiated iPSCs had converted into LMX1A/FOXA2-positive midbrain floor plate precursors, an early stage of mDA neuron development (Figure S3B). Immature mDA neurons at day 32 of differentiation were transiently treated with mitomycin C to eliminate remaining proliferating progenitors (Figure S3C). iPSC-mDA neurons that were matured for an additional 6 weeks (day 70) continued to express mDA markers such as FOXA2 and tyrosine hydroxylase (TH) in all iPSC clones independent of donor age (Figures S3D and S3E). Interestingly, iPSC-mDA neurons spontaneously showed evidence of low-level nuclear folding concomitant with the onset of endogenous lamin A expression (Figure S3F).

To achieve similar expression levels of progerin in iPSC-mDA neurons as in the iPSC-fibroblasts, we extended modified-RNA exposure to 5 days (Figure 4A), which induced progerin levels exceeding the levels of endogenous lamin A (Figure 4B, arrows). Following progerin overexpression, GFP+ cells showed evidence of enhanced nuclear folding and blebbing and accumulation of DNA damage (Figure 4C) and mtROS (Figure 4D). However, in contrast to iPSC-fibroblasts (Figure 3), we did not observe significant changes in LAP2α, H3K9me3, or HP1γ in neurons (Figure 4E). Positive SA-β-gal staining, a marker of senescence, was also not detected in iPSC-mDA neurons. These data demonstrate both shared and cell-type-specific responses of iPSC-fibroblasts and mDA neurons to our in vitro aging paradigm.

To further examine cell-type-specific responses to progerin exposure, we investigated parameters associated with neuronal aging in vivo such as degenerative changes in dendrite branching (Hof and Morrison, 2004). Remarkably, 5 days of progerin exposure in differentiated (day 65) mDA neurons was sufficient to induce a degenerative phenotype resulting in the breakdown of established neurites (Figure 5A). No degeneration was observed in cells transfected with nuclear-GFP mRNA. We next assessed expression of MAP2, which specifically labels dendrites (Bernhardt, 1984). Quantitative analysis showed a marked reduction in average dendrite length following progerin exposure in mDA neurons from both young and old donor iPSCs (Figure 5B). Importantly, the percentages of iPSC-mDA neurons expressing the dopamine neuron markers NURR1 and TH remained unchanged, suggesting that the addition of progerin did not simply induce toxicity (Figures S4A and S4B), in contrast to the treatment with mitochondrial toxins such as CCCP that rapidly induced mDA neuron marker loss (data not shown).

To further characterize the age-like phenotype in iPSC-mDA neurons following progerin overexpression, we performed gene expression analysis by RNA-seq. Principle component analysis confirmed a reset in gene expression following reprogramming and illustrated the similarity between iPSC-mDA neurons from donors of different ages (Figure 5C). Furthermore, progerin overexpression induced highly similar ($p < 2.93 \times 10^{-321}$) changes in young and old donor iPSC-mDA neurons (Figures 5C and S4C). Many of the overlapping progerin-induced expression changes (Figure S4C; Table S3) have been previously associated with processes involved in neuronal aging, including axon degeneration/regeneration (*TMSB10*, *TMSB4X*, *CCDC126*, *TSNAX*, *NOSTRIN*, and *LAMC3*), protein misfolding and aggregation (*NEDD8*, *PSMB3*, *PPIB*, and *UBC*), oxidative stress (*ENHO*, *NDUFB6*, *ATP5L*, *PRDX4*, *FTL*, *ATOX1*, and *TNIP3*), DNA damage (*NOP10* and *TCEAL7*), cell-cycle induction (*PCNA* and *MIR663A*), and chromatin modification (*PRDM1*) (Figure 5D). Induction of transcripts associated with age-like processes was confirmed by analysis of gene ontology (Figure S4D). Among the differentially expressed transcripts, we also found several uncharacterized genes and noncoding RNAs (Figure 5E) reminiscent of recent observations in the aging rat brain (Wood et al., 2013).

Progerin-Induced Aging Enables Modeling of Late-Onset PD Features In Vitro and In Vivo

A key motivation for manipulating age in iPSC-neurons is the need for developing faithful models of late-onset neurodegenerative disorders such as PD. Several groups have established

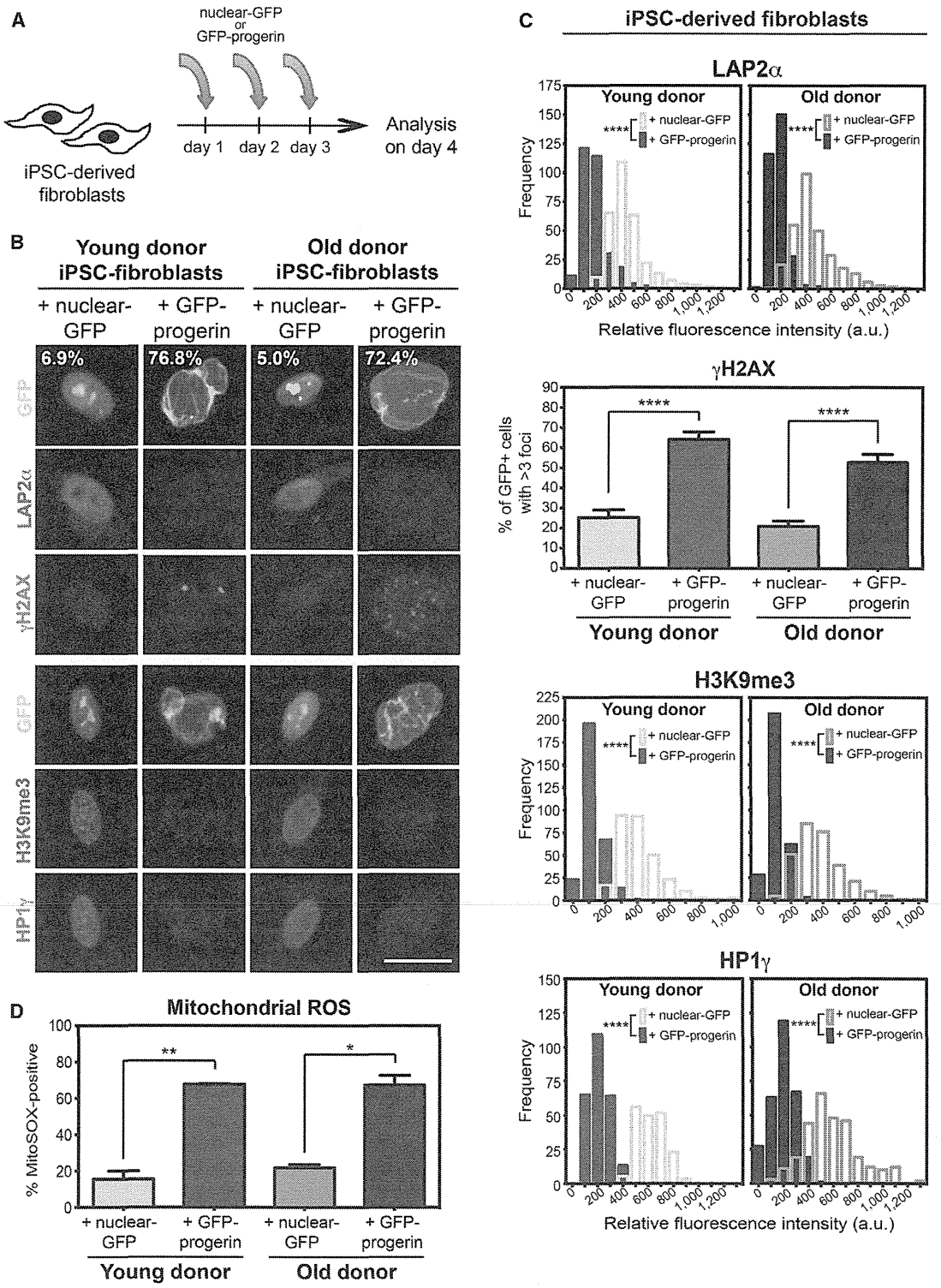

Figure 3. Progerin Overexpression Induces Age-Associated Changes in iPSC-Fibroblasts Regardless of Donor Age

(A) Modified-RNA was transfected into iPSC-fibroblasts on 3 consecutive days prior to analysis on day 4.

(B) Overexpression of progerin (GFP-progerin) in iPSC-fibroblasts causes changes in nuclear morphology (as seen by GFP), expression of the LAP (LAP2α), levels of DNA damage (γH2AX), and chromatin organization (H3K9me3; HP1γ), which were not observed with overexpression of a nuclear-GFP. Percentages indicate the proportion of cells with folded and/or blebbed nuclear morphologies. Scale bar, 25 μm.

(legend continued on next page)

iPSC-based disease models of PD. However, those studies reported phenotypes in cell types of uncertain relevance for PD such as neural stem cells (Liu et al., 2012b) or early biochemical phenotypes in mDA neurons without modeling the severe neurodegenerative features of the disease (Cooper et al., 2012; Nguyen et al., 2011; Seibler et al., 2011). We hypothesized that the lack of a neurodegenerative phenotype in those studies may be a result of the age reset during reprogramming. Similar to patients with PD who do not exhibit disease symptoms until later in life, PD iPSC-mDA neurons may be too "young" to mimic the degenerative phase of the disease. Therefore, we tested whether progerin overexpression may reveal disease-associated phenotypes that cannot be currently modeled in PD iPSC studies. We derived mDA neurons from PD iPSCs with homozygous mutations (Figure S5A; Table S2) in PINK1 (Q456X) or Parkin (V324A). PINK1 and Parkin are thought to act in a common pathway to promote the autophagic degradation of damaged mitochondria (Dodson and Guo, 2007), in addition to the unique functions of Parkin in the ubiquitin-proteasome pathway (Shimura et al., 2000).

PD iPSCs differentiated into mDA neurons with similar efficiencies than iPSCs from apparently healthy donors (C1 and C2; Figures S5B and S5C). Furthermore, PD and control iPSC-mDA neurons (day 65), transfected with GFP-progerin or nuclear-GFP for 5 days, did not show changes in NURR1 (Figure 6A) or TH (Figure 6B) expression. We were particularly interested in defining PD-related phenotypes that depend on induced in vitro aging and thereby mimic the late-onset nature of the disease. For instance, we observed a significant increase in condensed nuclei that expressed cleaved caspase-3 in PD versus control iPSC-mDA neurons (Figure 6C), indicating that PD mutant mDA neurons are more prone to activating a cell death program upon induced aging. GFP-progerin-positive condensed nuclei were not detected until day 4 or day 5 of progerin transfection, suggesting a progressive decline rather than an acute toxicity. Dendrite length in mDA neurons was not significantly affected in PD versus control iPSC-mDA neurons under control conditions. However, following progerin overexpression, loss of dendrite length was significantly enhanced in mDA neurons derived from PINK1-Q456X and Parkin-V324A iPSCs versus control iPSC-mDA neurons (Figures 6D and 6E).

It has been suggested that decreased neuronal survival in PD is in part caused by diminished levels of phosphorylated S473 AKT (p-AKT), based on studies in PD models (Malagelada et al., 2008; Tain et al., 2009) and in brain tissues from patients with sporadic PD (Timmons et al., 2009). Interestingly, PINK1-Q456X and Parkin-V324A mutant iPSC-mDA neurons showed a significant reduction in p-AKT in response to progerin, whereas C1 and C2 iPSC-mDA neurons showed a slight increase in p-AKT (Figures 6F and 6G). The deregulation of AKT signaling also resulted in the corresponding changes in the phosphorylation of the downstream signaling targets ULK1 and 4EBP1 (Figures 6F and 6G). There was considerable variability in the basal levels of AKT, ULK1, and 4EBP1 across replicate differentiations independent of genotype and treatment (Figures 6F and S5D). However, the progerin-induced reduction in the activation status of AKT signaling components was consistent (independent of basal levels) and mimicked the reported signaling changes in PD.

To further confirm the progerin-induced differences between PD and control iPSC-mDA neurons, we reprogrammed additional fibroblasts from a patient with PD with a heterozygous R275W Parkin mutation using Sendai virus-based reprogramming. Similar to the progerin-induced phenotype in PINK1-Q456X and Parkin-V324A, progerin overexpression drove increased apoptosis (Figure 6C), enhanced dendrite shortening (Figure 6E), and reduced AKT activation (Figure S5E) in Parkin-R275W iPSC-mDA neurons compared to control iPSC-mDA neurons (C3 and C4).

In order to assess the long-term effects of progerin exposure, mDA neurons derived from PD and control iPSCs were transduced with lentiviral vectors expressing *GFP-progerin* or *nuclear-GFP* under the control of the neuron-specific human *synapsin* (*hSyn*) promoter and grafted into the striatum of 6-hydroxydopamine lesioned *NOD-SCID IL2Rgc*-null mice (Figure 7A). In vitro analysis of matched aliquots of cells 24 hr after transplantation confirmed expression of NURR1 and TH in GFP+ cells (Figure S6A). Onset of hSyn-driven transgene expression in vitro was detectable 1 day prior to grafting, and expression was maintained in cultured cells for at least 90 days (latest time point tested). In vivo analysis 3 months after grafting resulted in a reduction of amphetamine-induced rotation scores in most animals (Figure 7B), indicating mDA neuron survival above the threshold required for behavioral improvement. Interestingly, the subset of animals that did not recover (Figure 7B, pink symbols) had received either PINK1- or Parkin-derived neurons expressing progerin. Lack of recovery was surprising considering that survival of only few mDA neurons is required to rescue behavior. To address whether incomplete behavioral recovery in the animals was due to a smaller number of surviving mDA neurons, we performed stereological quantification of the grafts. Although graft volume was not significantly affected in progerin-treated versus control groups (data not shown), progerin-expressing mDA neuron grafts showed a dramatic reduction in TH^+ cell numbers (Figures 7C and 7D). Strikingly, the reduction in TH^+ cells was particularly pronounced in progerin-expressing mDA neuron grafts from PINK1-Q456X and Parkin-V324A iPSCs and minimal in control iPSC-mDA neuron grafts. Those results mimic the accelerated loss of TH observed in patients with PD, though the mechanism of TH^+ cell loss in the current study remains to be determined.

To further assess biomarkers of age and disease status of the iPSC-mDA neurons, we performed ultrastructural analysis of the

(C) Quantification of data shown in (B) is presented. Frequency distribution plots represent the fluorescence intensity of 100 cells from three independent RNA transfections of iPSC-fibroblasts derived from independent iPSC clones.

(D) Flow cytometry analysis of the mitochondrial superoxide indicator MitoSOX suggests a dramatic increase in mitochondrial dysfunction with progerin overexpression (n = 3 independent RNA transfections of iPSC-fibroblasts derived from independent iPSC clones).

*$p < 0.05$, **$p < 0.01$, and ****$p < 0.0001$, according to Kolmogorov-Smirnov tests (LAP2α, H3K9me3, and HP1γ) or Student's t tests (γH2AX and MitoSOX). Bar graphs represent mean ± SEM.

See also Figures S2 and S7, and Tables S2, S4, and S5.

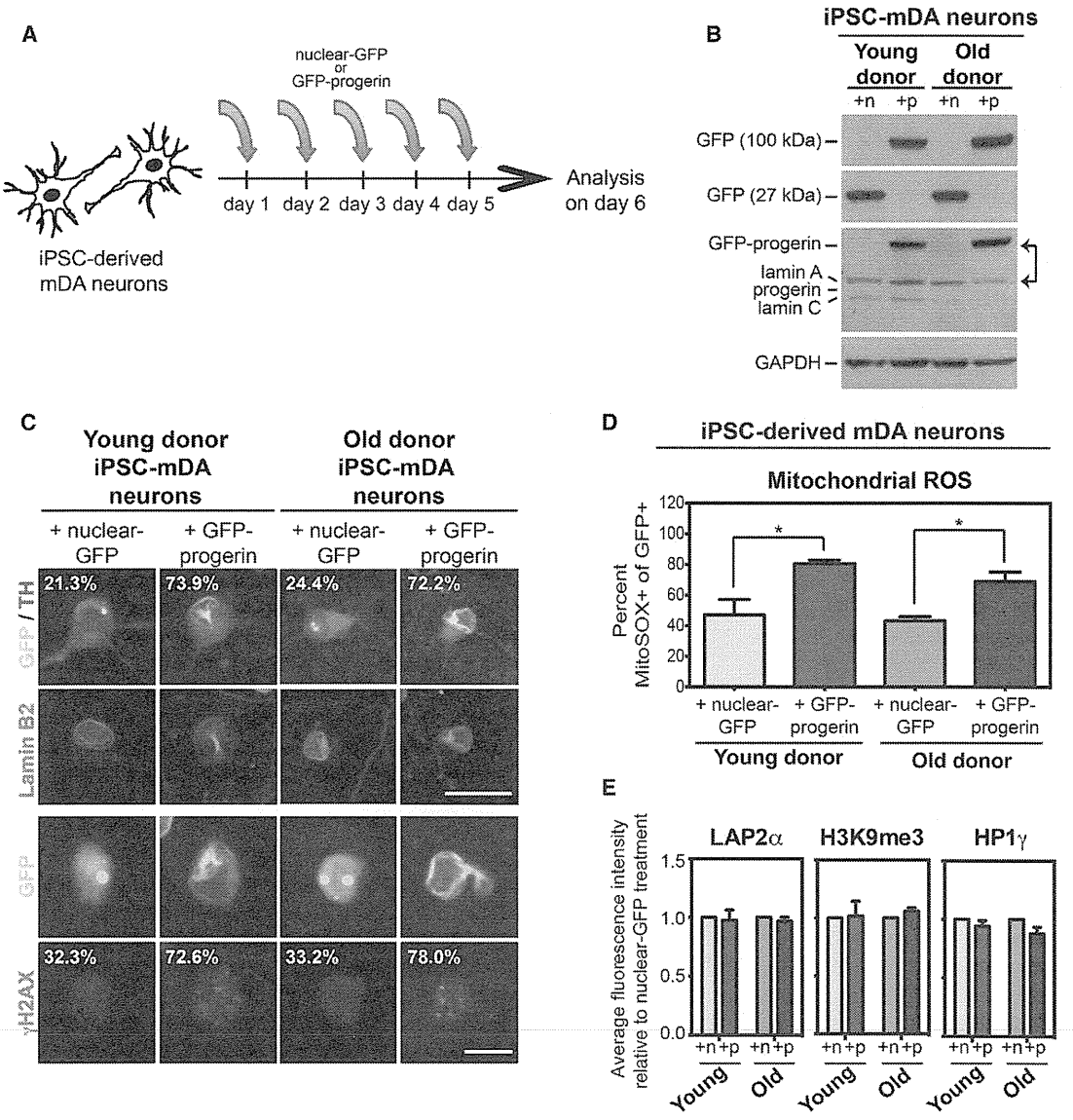

Figure 4. Progerin Overexpression Induces a Subset of the Fibroblast Age-Associated Signature in iPSC-mDA Neurons Derived from Both Young and Old Donors

(A) Modified-RNA was transfected into iPSC-mDA neurons on 5 consecutive days prior to analysis on day 6.

(B) Western blot analysis of transgene expression is shown. A GFP band at 100 kDa denotes the GFP-progerin (+p) fusion protein, whereas a GFP band at 27 kDa represents the nuclear-GFP (+n) transgene. All lamin A isoforms including the transgene were recognized by a single antibody. Note that progerin overexpression levels exceed endogenous lamin A levels (arrows). iPSC-mDA neurons do not appear to express detectable levels of progerin protein endogenously.

(C) Progerin overexpression enhances nuclear folding and blebbing (as seen by lamin B2, pink) and increases DNA-damage accumulation (γH2AX) in both young and old donor-derived iPSC-mDA neurons. Percentages indicate the proportion of cells with enhanced nuclear folding and/or blebbing or the proportion of cells with greater than three enlarged γH2AX foci. Scale bars, 10 μm (bottom) and 25 μm (top).

(D) Flow cytometry analysis of mitochondrial superoxide levels (MitoSOX) demonstrates increased mitochondrial dysfunction with progerin overexpression ($n = 3$ independent RNA transfections of iPSC-mDA neurons derived from independent iPSC clones). *$p < 0.05$, according to Student's t tests.

(E) Quantification of immunocytochemistry for LAP2α, H3K9me3, and HP1γ shows no difference between iPSC-mDA neurons transfected with GFP-progerin or nuclear-GFP, unlike the phenotype observed in iPSC-fibroblasts (see Figure 3). Fluorescence intensities were normalized to the intensities observed in nuclear-GFP-treated cells.

Bar graphs represent mean ± SEM.

See also Figures S3 and S7, and Tables S2, S4, and S5.

grafts 6 months after transplantation by transmission electron microscopy (TEM). Initial observations by light microscopy demonstrated a continued, progressive loss of TH immunoreactivity in grafts overexpressing progerin (Figure S6B). Analysis by TEM confirmed the progerin-induced reduction of TH expression in iPSC-mDA neuron dendrites and folded nuclear

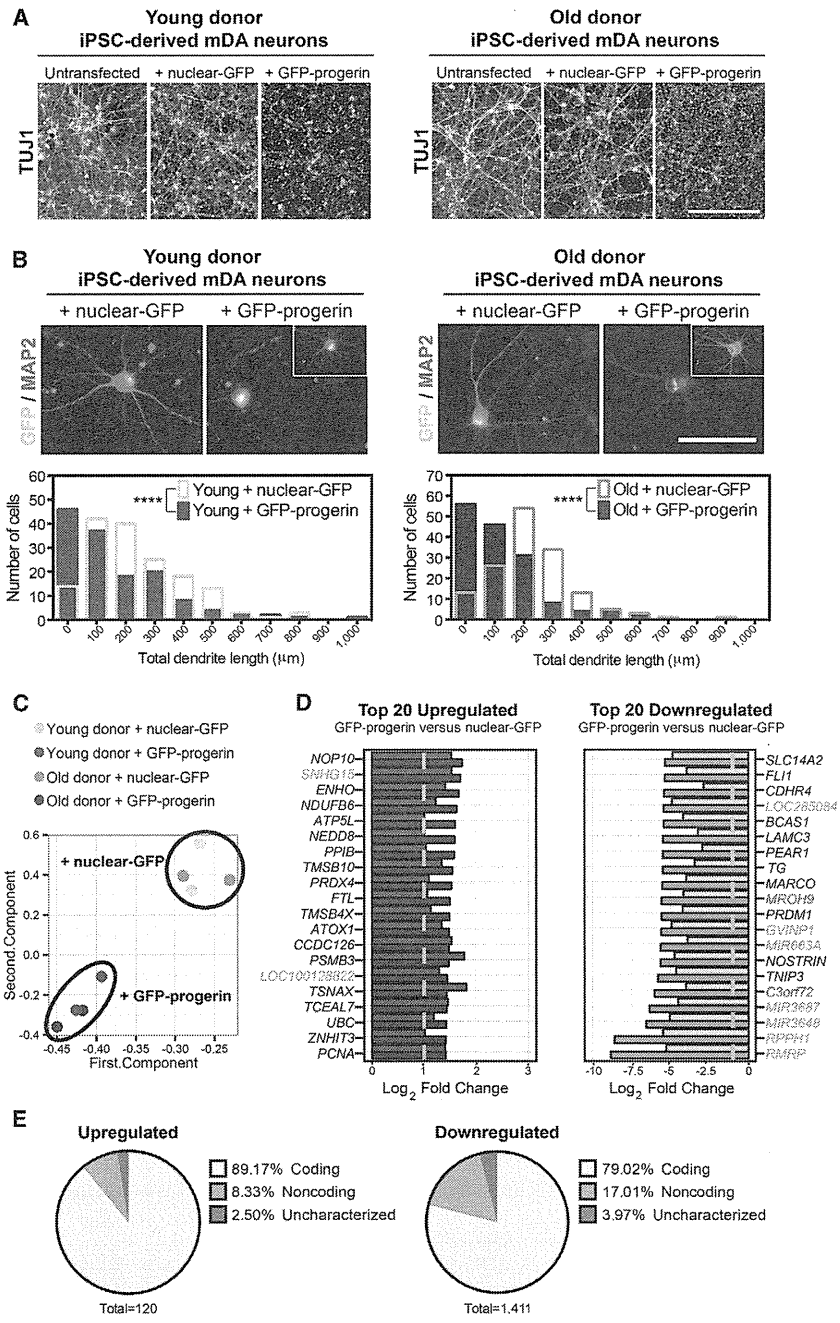

Figure 5. Progerin Overexpression Elicits Features Consistent with Neuronal Aging in iPSC-mDA Neurons

(A) Immunocytochemistry for the pan-neuronal marker TUJ1 shows a loss of the established neuronal network in day-70 iPSC-mDA neurons overexpressing progerin, but not iPSC-mDA neurons overexpressing nuclear-GFP. Scale bar, 200 μm.

(B) MAP2 immunocytochemistry reveals reduced intact dendrite lengths following overexpression of progerin in most but not all (insets) iPSC-mDA neurons derived from both young and old donors. Frequency distributions display total dendrite length measurements from three independent RNA transfections (50 cells each, nonapoptotic nuclei only). Scale bar, 50 μm. ****$p < 0.0001$, according to Kolmogorov-Smirnov tests.

(C) Principal component analysis of RNA-seq gene expression data further corroborates the reprogramming-induced reset of age that results in the high similarity of iPSC-mDA neurons from both young and old donors. Progerin overexpression induces similar changes in mDA neurons independent of donor age.

(D) The top 20 upregulated (left) and downregulated (right) genes in progerin-treated compared to control nuclear-GFP-treated young donor (green) and old donor (blue) iPSC-mDA neurons are shown. Genes are ranked according to iPSC-mDA neurons derived from the old donor. Red denotes uncharacterized genes, and orange denotes noncoding RNAs. Dotted line indicates the threshold for significance.

(E) Pie charts represent the proportion of the significantly differentially expressed transcripts that are coding, noncoding, or uncharacterized. See also Figures S4 and S7, and Tables S2, S3, S4, and S5.

morphologies (Figures S6C and S6D). To determine the age status of the grafted neurons, we focused on the intracellular accumulation of neuromelanin. Neuromelanin is a dark-colored pigment present in adult mDA neurons but absent in fetal or neonatal stages including iPSC-mDA neurons (Mann and Yates, 1974; Sulzer et al., 2008). In human fetal tissue transplantation studies, neuromelanin was detected in grafts 4–14 years after intrastriatal injection, a time course similar to normal development (Loh et al., 2010). In just 6 months, we observed robust accumulation of neuromelanin with lipofuscin deposits selectively in grafts overexpressing progerin (an average of eight deposits per 55 μm^2 versus 0.5 in control nuclear-GFP-expressing grafts, Figure 7E) and regardless of genetic background.

In addition, progerin overexpression revealed genotype-specific effects in PD iPSC-derived grafts, phenotypes not observed in PD grafts overexpressing nuclear-GFP, or in any non-PD control grafts. For instance, signs of neurite degeneration such as the appearance of fibrillar bodies were prominent in PD-derived grafts overexpressing progerin (asterisks in Figures 7E, 7G, and S6C), indicating a breakdown of microtubules (Jaworski et al., 2011). Furthermore, PINK1-Q456X grafts contained cells with enlarged mitochondria, a phenotype much more pronounced in progerin-overexpressing cells (area of 0.167 μm^2 compared to 0.0387 μm^2 for PINK1 plus nuclear-GFP; $p = 0.0005$; Figures 7F and S6F). In contrast, Parkin mutant grafts showed less-dramatic mitochondrial defects (such as abnormal mitochondrial fusion; data not shown) but, strikingly, exhibited large multilamellar inclusions (Figure 7G). Multilamellar inclusions have been observed in various neurodegenerative models

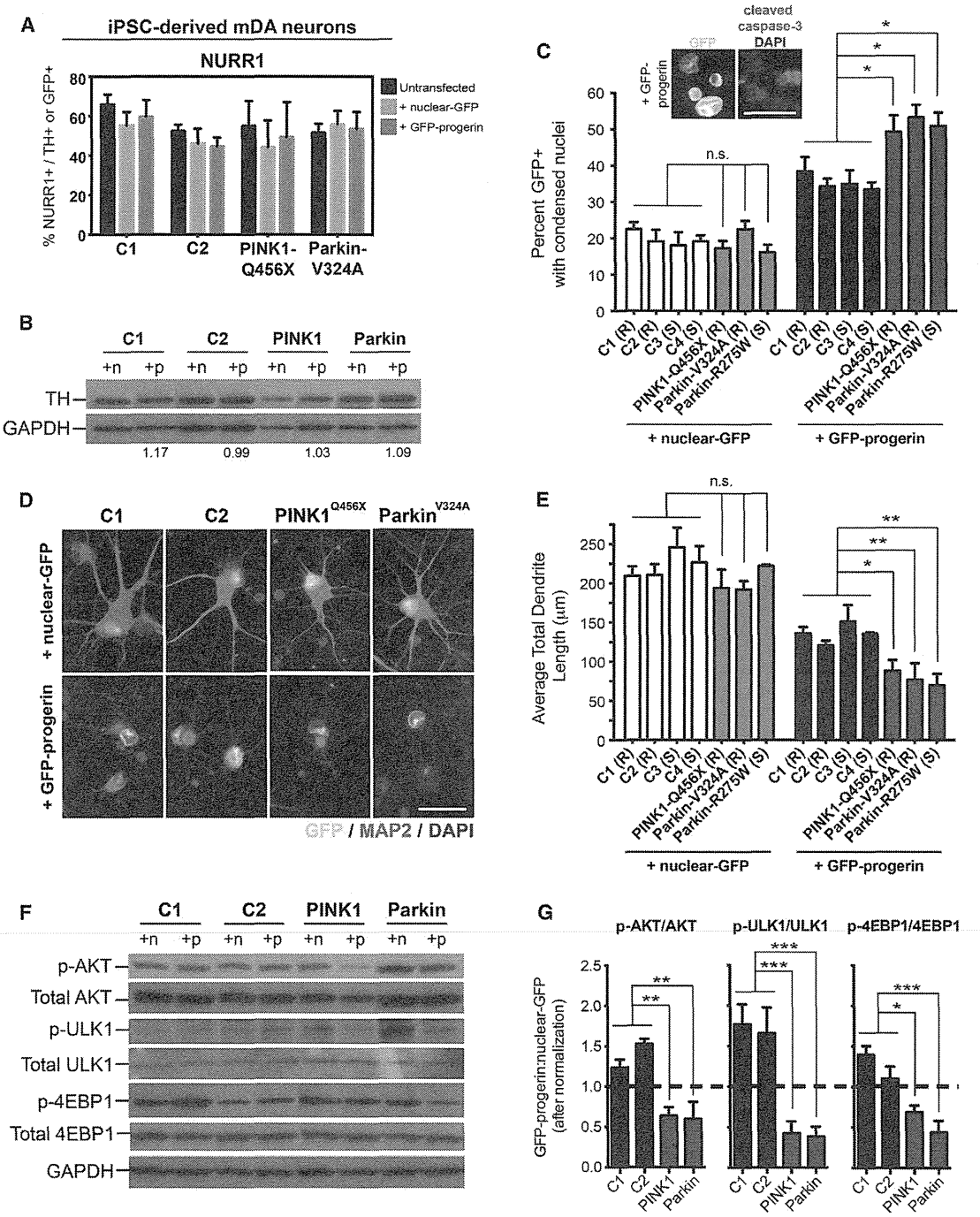

Figure 6. Progerin Overexpression Reveals Disease-Specific Phenotypes In Vitro in iPSC-Based Models of Genetic PD

(A and B) Quantification of NURR1+ cells (A) and western blot analysis of TH protein levels (B) do not reveal significant differences with transfection of GFP-progerin (+p) modified-RNA. +n, nuclear-GFP. Numbers below the western blot indicate the ratio of GFP-progerin:nuclear-GFP expression of TH normalized to GAPDH.

(C) Analysis of GFP+ cells undergoing cell death following RNA transfection as identified by condensed nuclear morphologies is shown. Images display a representative example of cleaved caspase-3 immunocytochemistry in cells treated with progerin.

(D) Immunocytochemistry for the dendrite marker MAP2 is shown.

(E) Quantification of total dendrite lengths per GFP+ neuron shows accelerated dendrite shortening in PD mutant iPSC-mDA neurons compared to apparently healthy controls (C1–C4) in response to progerin overexpression.

(F and G) Western blot analysis of AKT pathway signaling (F) demonstrates genotype-specific responses to progerin overexpression. For quantification, phospho-specific bands (G) were normalized to total protein before calculating the ratio of the levels expressed following progerin versus nuclear-GFP treatment.

(legend continued on next page)